the plant journal

SEB Society for Experimental Biology

The Plant Journal (2011) **67**, 381–394 doi: 10.1111/j.1365-313X.2011.04601.x

Mutational analysis of Arabidopsis chloroplast polynucleotide phosphorylase reveals roles for both RNase PH core domains in polyadenylation, RNA 3′-end maturation and intron degradation

Arnaud Germain[1], Shira Herlich[2], Shirley Larom[2], Sang Hu Kim[1], Gadi Schuster[2] and David B. Stern[1,*]

[1]*Boyce Thompson Institute for Plant Research, Tower Road, Ithaca, NY 14853, USA, and*

[2]*Faculty of Biology, Technion-Israel Institute of Technology, Haifa 32000, Israel*

Received 15 February 2011; revised 28 March 2011; accepted 4 April 2011; published online 25 May 2011.

*For correspondence (fax +607 254 6779; e-mail ds28@cornell.edu).

SUMMARY

Polynucleotide phosphorylase (PNPase) catalyzes RNA polymerization and 3′ → 5′ phosphorolysis *in vitro*, but its roles in plant organelles are poorly understood. Here, we have used *in vivo* and *in vitro* mutagenesis to study Arabidopsis chloroplast PNPase (cpPNPase). In mutants lacking cpPNPase activity, unusual RNA patterns were broadly observed, implicating cpPNPase in rRNA and mRNA 3′-end maturation, and RNA degradation. Intron-containing fragments also accumulated in mutants, and cpPNPase appears to be required for a degradation step following endonucleolytic cleavage of the excised lariat. Analysis of poly(A) tails, which destabilize chloroplast RNAs, indicated that PNPase and a poly(A) polymerase share the polymerization role in wild-type plants. We also studied two lines carrying mutations in the first PNPase core domain, which does not harbor the catalytic site. These mutants had gene-dependent and intermediate RNA phenotypes, suggesting that reduced enzyme activity differentially affects chloroplast transcripts. The interpretations of *in vivo* results were confirmed by *in vitro* analysis of recombinant enzymes, and showed that the first core domain affects overall catalytic activity. In summary, cpPNPase has a major role in maturing mRNA and rRNA 3′-ends, but also participates in RNA degradation through exonucleolytic digestion and polyadenylation. These functions depend absolutely on the catalytic site within the second duplicated RNase PH domain, and appear to be modulated by the first RNase PH domain.

Keywords: chloroplast, intron, RNA, polynucleotide phosphorylase, ribonuclease, splicing.

INTRODUCTION

Polynucleotide phosphorylase (PNPase) is present in organelles and many bacteria, and was first defined as a reversible polynucleotide polymerase (Grunberg-Manago and Ochoa, 1955), a property shared by the spinach chloroplast enzyme (Yehudai-Resheff *et al.*, 2001). The degradative activity of PNPase is processive 3′ → 5′ phosphorolysis, and the chloroplast enzyme is capable of trimming 3′-end extensions to near the base of stem-loop structures *in vitro* (Yehudai-Resheff *et al.*, 2001). Similarly, Arabidopsis plants depleted for (Walter *et al.*, 2002) or lacking (Marchive *et al.*, 2009) chloroplast PNPase (cpPNPase) accumulate several mRNAs as well as 23S rRNA with 3′ extensions. Higher plants also encode a mitochondrial PNPase (mtPNPase), which is essential for embryo development. Depletion of mtPNPase revealed its involvement in both mRNA and rRNA maturation and degradation (Perrin *et al.*, 2004a,b). Furthermore, mtPNPase degrades noncoding RNA sequences that result from relaxed transcription (Holec *et al.*, 2006).

The polymerization activity of PNPase may have two independent roles in chloroplasts. First, the addition by PNPase of poly(A)-rich tails to RNAs lacking 3′ secondary structures can stimulate 3′ → 5′ exonucleolytic resection and ultimately RNA degradation (reviewed in Schuster and Stern, 2009). Indeed, *Chlamydomonas* cells depleted for cpPNPase appear to lack chloroplast polyadenylation (Zimmer *et al.*, 2009). On the other hand, in Arabidopsis it was reported that depletion of cpPNPase led to an increase in poly(A) tail amount (Walter *et al.*, 2002). This finding suggests that higher plant chloroplasts, like bacteria, also

utilize a poly(A) polymerase (PAP). Second, poly(A) tail addition to RNAs with strong secondary structures may stimulate mRNA 3′-end maturation, as suggested by the cloning of polyadenylated *Chlamydomonas atpB* cDNAs with the tail added at a pre-mRNA processing site (Komine *et al.*, 2000).

A number of studies have also revealed intriguing roles for PNPase in cellular functions not directly related to RNA metabolism. For example, *Chlamydomonas* cells depleted for cpPNPase cannot survive phosphorus deprivation (Yehudai-Resheff *et al.*, 2007), and the orthologous Arabidopsis mutant fails to elaborate lateral roots under the same growth condition (Marchive *et al.*, 2009). An Arabidopsis cpPNPase null mutant was also identified in a screen for mutants resistant to fosmidomycin, an inhibitor of the methylerythritol phosphate pathway (Sauret-Gueto *et al.*, 2006). In human mitochondria, PNPase is found in the intermembrane space (Chen *et al.*, 2006), separate from the location of mtRNA, yet its depletion somehow alters mtRNA metabolism (Slomovic and Schuster, 2008). Furthermore, a recent study implicated mtPNPase in the import of small RNAs into human mitochondria (Wang *et al.*, 2010). Clearly, PNPase functions in a diverse array of cellular pathways.

Although PNPase has emerged as a central player in RNA metabolism and other activities, systematic structure-function analysis of cpPNPase has been so far very limited (Yehudai-Resheff *et al.*, 2003). PNPase consists of tandem N-terminal RNase PH-like segments, known as core domains, as well as KH and S1 RNA-binding domains (Figure 1a). RNase PH is an exoribonuclease (Deutscher, 1993), however PNPase crystal structures from *Streptomyces antibioticus* and *E. coli*, along with a comparison to the archaeal exosome, suggested that only the second core domain would harbor catalytic activity (Lorentzen *et al.*, 2005; Nurmohamed *et al.*, 2009; Symmons *et al.*, 2000). Indeed, the initial observation of catalytic activity for the first core of spinach cpPNPase (Yehudai-Resheff *et al.*, 2003) was not supported by subsequent experiments (G. Schuster, Technion-Israel Institute of Technology, Haifa, Israel, unpublished results). Here, we have taken a mutagenesis approach to study Arabidopsis cpPNPase, using both null mutants and point mutants. We found massive disruptions in transcript patterns, and a substantial accumulation of complete or partial intron lariats. We also found two mutations in the first core domain that lead to RNA abnormalities, one of which confers altered PNPase properties *in vitro*, confirming a role for this domain in PNPase catalytic activity.

RESULTS

Phenotypes of *PNPase* T-DNA insertion and single amino acid mutants

To study cpPNPase function, we used both the previously-described T-DNA insertion mutants *pnp1-1* and *pnp1-2*

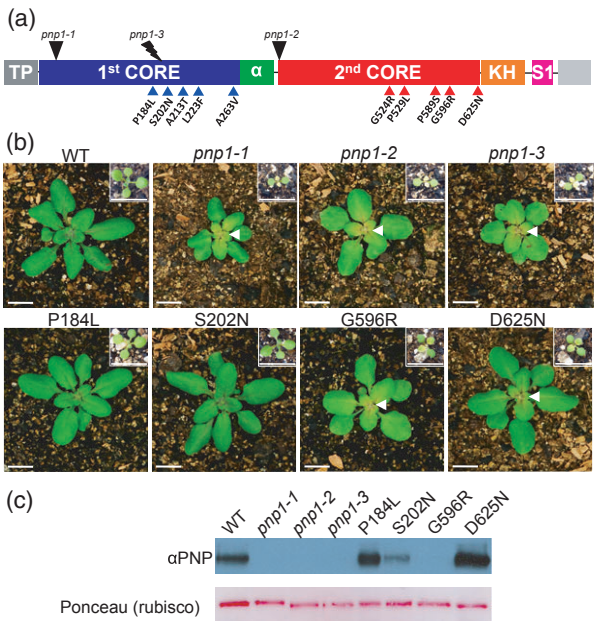

Figure 1. Identification of Arabidopsis *pnp* mutants.
(a) Domain structure of Arabidopsis cpPNPase. TP indicates the chloroplast transit peptide, α represents the α-helical domain and the gray C-terminal domain is an extension unique to cpPNPase. Black arrowheads indicate T-DNA insertions (*pnp1-1* and *pnp1-2*), the black lightning bolt indicates a premature translation termination codon caused by a single nucleotide substitution at a splice junction (*pnp1-3*), and the blue and red arrowheads indicate single amino acid substitutions resulting in amino acid changes in the first and the second core domains, respectively.
(b) Phenotypes of a Col-0 wild-type plant (WT) and selected mutants. The white arrowheads point to the pale green emerging leaves. The white bar represents 1 cm.
(c) Immunoblot analysis using a cpPNPase-specific antibody on plastid soluble protein-enriched samples from the WT and mutants. Samples were loaded in a Blue Native gel based on protein concentration, as reflected in Ponceau-S staining of the membrane.

(Marchive *et al.*, 2009), and 11 additional point (TILLING) mutants (Till *et al.*, 2003). One of the TILLING mutants was shown to generate a premature stop codon at position 600 (Figure 1a), and was designated *pnp1-3*. The other 10 point mutations, five in each core domain, all caused amino acid alterations, and were selected based on the conservation of that amino acid amongst chloroplast, mitochondrial and bacterial PNPases (see Figure 7 in Yehudai-Resheff *et al.*, 2003).

Figure 1(b) only shows images of mutants that had growth and/or RNA abnormalities, as is the case in subsequent figures. The null mutants (*pnp1-1*–*pnp1-3*) as well as G596R and D625N have similar growth phenotypes, in that their first true leaves (Figure 1b, insets) and subsequent new leaves emerge pale green (Figure 1b), but recover as they mature. Growth of two other mutants that were later found to have milder RNA phenotypes, P184L and S202N, did not differ from the WT.

PNPase accumulation was monitored by Blue Native gel electrophoresis and immunoblot (Figure 1c), revealing

a signal at 600 kDa, the expected size for the PNPase hexamer (Baginsky *et al.*, 2001), and confirming its absence in the three null mutants. Of the TILLING mutants, D625N appeared to overaccumulate PNPase, P184L was comparable to the WT, S202N slightly lower than the WT, and for G596R, no signal could be detected in either native or denaturing gels. Because qRT-PCR showed that the G596R *PNP* transcript accumulated to about 40% of the WT level (data not shown), we conclude that this substitution compromises PNPase stability.

Both PNPase domains contribute to chloroplast rRNA and mRNA processing

To confirm earlier findings for cpPNPase-depleted plants, and extend them to the point mutants studied here, total RNA was first examined by gel electrophoresis and ethidium bromide staining, revealing a reduced mobility for one of the fragments comprising chloroplast 23S rRNA for the three null mutants, as well as G596R and D625N (Figure S1). This is due to defective exonucleolytic trimming of approximately 100 nucleotides (nt) of the intergenic region between 23S and 4.5S rRNA (Walter *et al.*, 2002). Because G596R lacks cpPNPase (Figure 1c), and because D625N resembled *pnp1-1* to *pnp1-3* in this and all subsequent experiments, the five mutants will henceforth be referred to collectively as the null mutants. An intermediate phenotype was observed for P184L, in which a conserved residue located in the phosphorolytically inactive first core domain is altered. In this case, a mixture of mature and 3′-extended 23S rRNA was observed. Thus, with respect to 23S rRNA maturation, P184L is a weak *pnp* mutant allele; the other mutants appeared as the WT.

We also confirmed (Figure S2a) previously published 3′ extensions for the monocistronic *rbcL* and *psbA* transcripts (Marchive *et al.*, 2009), which in the case of *rbcL* was verified by gel blot (Figure S2b). Again, a mixture of the WT and null mutant pattern was observed for P184L. In addition, we examined the dicistronic *atpB-atpE* gene cluster (Figure S2c), whose slightly more complex transcript pattern derives from the presence of two promoters as well as processing to yield *atpE*-specific species (Schweer *et al.*, 2006). Again, the pattern was interpretable as 3′-end extensions although in this case, P184L appeared as the WT. This finding suggests that *atpBE* 3′-end maturation is less sensitive to the amount of cpPNPase activity.

Analysis of polycistronic gene clusters reveals gene-dependent patterns for both coding and intronic regions

The Arabidopsis chloroplast genome encodes several intron-containing polycistronic gene clusters. We analyzed two such clusters, namely those encoding *atpI*/*atpH*/*atpF*/*atpA* and *psbB*/*psbT*/*psbN*/*psbH*/*petB*/*petD*. For the *atpI* gene cluster (Figure 2), a molecular phenotype common to null mutants for all five probes used is the presence of non-discrete high molecular transcripts that correlate with the diminution of most of the corresponding discrete bands (Figure 2b). These may represent imprecise 3′-end formation rather than transcript instability. Indeed, qRT-PCR analysis of the *atpI* coding region showed no difference between the WT and *pnp1-1* (data not shown), although only the band marked ‘1’ remains discrete and unchanged. Even though we did not quantify the *atpA* or *atpF* coding region transcripts, the gel patterns are consistent with a similar conclusion; i.e. that no significant accumulation differences occur in the null mutant backgrounds.

Also of note were four novel bands observed for *atpH* (marked 2–5). Bands 2 and 5 were present only in the null mutants, band 3 was prominent in the null mutants and P184L, and present weakly in another mutant of the first core domain, S202N. Band 4 was present in all mutants, but most strongly in the weak allele P184L. One possible interpretation could be that bands 2–5 represent the products of a succession of endonucleolytic cleavages between *atpH* and *atpF* that are subsequently trimmed by PNPase. This situation would be consistent with a recently proposed model for chloroplast polycistronic RNA processing (Pfalz *et al.*, 2009). Their reduced intensities in the weak alleles probably reflect the presence of residual cpPNPase activity in those mutants. In the case of band 4, however, the residual activity increases its abundance perhaps, for example, by trimming band 2 or 3. The precise 3′-ends of *atpH* transcripts were compared between the WT and *pnp1-1* using circular RT-PCR (cRT-PCR; Figure 2c). WT transcripts had two main 3′-ends. The end nearest the coding region was well represented in *pnp1-1*, suggesting it might be generated by transcription termination. The *pnp1-1* mutant also accumulated a series of extended 3′-ends, as suggested by the gel blot, and in keeping with the possibility that they are endonucleolytic cleavage products.

In the *psbB* gene cluster (Figure 3), two genes (*petB* and *petD*) contain introns, while *psbN* is expressed from its own promoter on the opposite strand. As shown in Figure 3(b), the various coding region probes, with the exception of *psbN*, revealed patterns that while more complex, were reminiscent of other genes described above, with the null mutants showing stronger effects, and P184L and S202N intermediate phenotypes. On the other hand, transcripts appeared to be less diffuse than in the case of the *atpI* cluster (Figure 2), suggesting that their 3′-ends might be more homogeneous. We checked this by cRT-PCR, using *petD* as an example (Figure 3c), and found that although it had multiple 3′-ends, they were indeed less dispersed than for *atpH* (Figure 2c). In the case of *psbN*, the null mutants were nearly depleted for the transcript (Figure 3b) which, however, is dispensable for normal PSII function (Zghidi *et al.*, 2007). In addition, for *psbB* a band shorter than any WT transcript was observed (band 1), which we speculate is a degradation intermediate. The hybridization patterns for the intron probes are discussed in the next section.

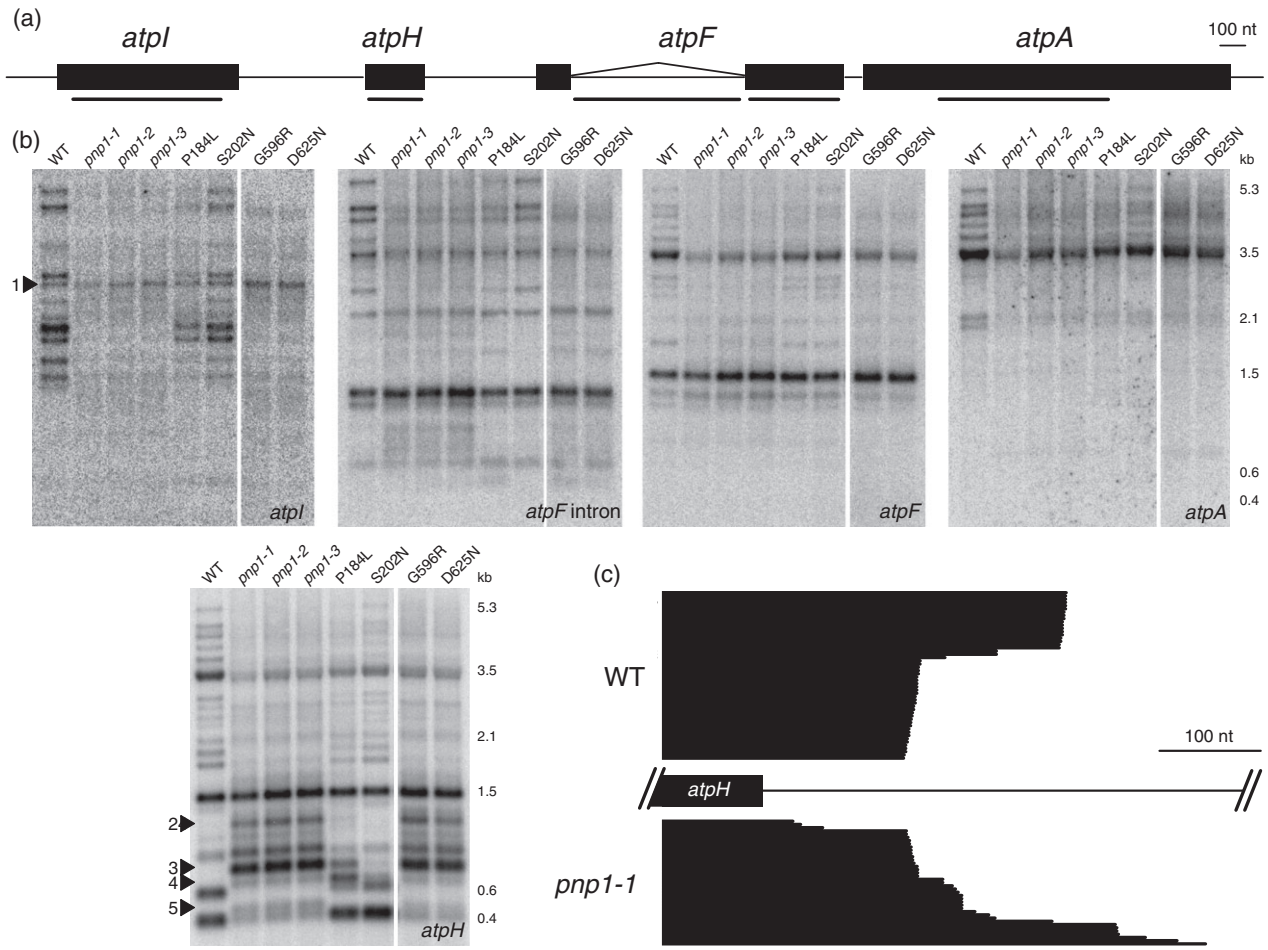

Figure 2. Analysis of the *atpI*/*atpH*/*atpF*/*atpA* gene cluster.
(a) Diagram of the *atpI*/*atpH*/*atpF*/*atpA* gene cluster and locations of the probes used for RNA gel blot analysis (black bars).
(b) Results for the five specific probes as indicated at the bottom right of each panel. The numbered arrowheads refer to specific transcripts discussed in the text.
(c) Schematic of cRT-PCR results showing *atpH* 3′-ends for WT and *pnp1-1*, with each horizontal line corresponding to a single clone. The number of clones sequenced for WT and *pnp1-1* was 52 and 39, respectively.

Ultimately, a variety of other transcripts examined in the PNPase mutants showed a range of effects, including apparent 3′-end extensions, accumulation of putative degradation intermediates, and instances where no transcript alterations were detected. Also, several other intron probes revealed mutant-specific bands possibly analogous to the one studied in detail below for *petD*. These data are presented in Figure S3.

PNPase depletion decreases splicing efficiency and inhibits intron degradation

We were particularly intrigued by the hybridization patterns for the *petB* and *petD* introns (Figure 3b), in which bands shorter than the complete excised introns (bands 2 and 4) were detected, these being band 3 for the *petB* intron and bands 5 and 6 for the *petD* intron. Given these results, we suspected that *pnp* mutants had a defect in some aspect of intron removal or degradation. To measure splicing efficiency, we used poisoned primer extension, and found that a 1.5- to twofold change in the ratio of spliced to unspliced RNA occurs in all the null mutants (Figure 4a). This relatively small reduction in splicing, however, would not appear to explain the high accumulation of intron-containing fragments.

The introns discussed here belong to Group II, whose splicing mechanism entails lariat formation (reviewed in Stern *et al.*, 2010). The amount of the lariat junction can be measured by qRT-PCR using two primers pointing towards the junction, and Figure 4(b) shows results for the amount of lariat junction-containing *petD* intron fragments in the WT and null mutants. While there was some variability, each mutant accumulates four to eightfold more lariat junctions than the WT. This suggests that the *pnp*-specific intron-containing bands 5 and 6 in Figure 3(b) include the lariat

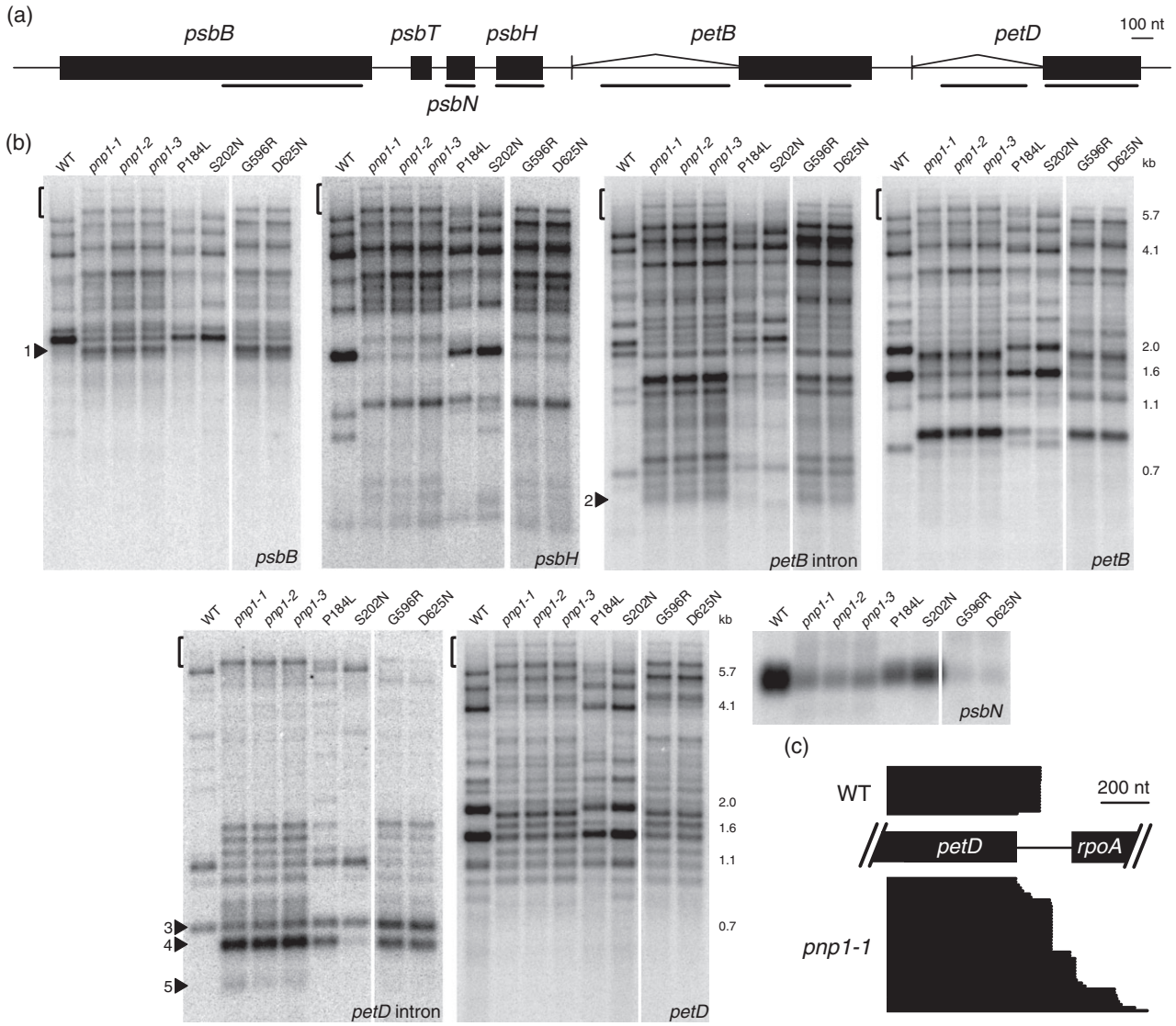

Figure 3. Analysis of the *psbB*/*psbT*/*psbN*/*psbH*/*petB*/*petD* gene cluster.
(a) Diagram of the *psbB*/*psbT*/*psbN*/*psbH*/*petB*/*petD* gene cluster and locations of the probes used for RNA gel blot analysis (black bars).
(b) Results for the seven specific probes as indicated at the bottom right of each panel. The numbered arrowheads refer to specific transcripts discussed in the text. Note that *psbN* is on the opposite strand.
(c) Schematic of cRT-PCR results showing *petD* 3′-ends for WT and *pnp1-1*, with each horizontal line corresponding to a single clone. The number of clones sequenced for WT and *pnp1-1* was 16 and 44, respectively.

junction, and because they are shorter than the full-length excised intron (band 4), represent intron degradation intermediates.

We subsequently decided to focus on band 5, the most abundant novel intron-containing band in the null mutants. To map its ends we used cRT-PCR. As shown in the Figure 5 inset, samples not treated with T4 RNA ligase gave rise to amplification of the intact intron (open arrowhead), as expected. However, ligated samples generated additional bands (full arrowheads), with a major *pnp1-1* product absent from the WT sample, suggesting that it might represent the gel band of interest from Figure 3(b). A faint and smaller band was amplified in the WT. Both products were cloned and sequenced, and although their ends were variable (see below), the WT and *pnp1-1* products lacked approximately 240 and 200 nt, respectively, in comparison with the 709-nt full-length intron.

Figure 5 shows a model of the *petD* intron upon which the 5′- and 3′-ends of cRT-PCR products are displayed. The cloned 5′-ends were similar in the WT and *pnp1-1*, with most being clustered in a 6-nt stretch in the first stem of Domain I, and most of the remaining ones in the loop of Domain II.

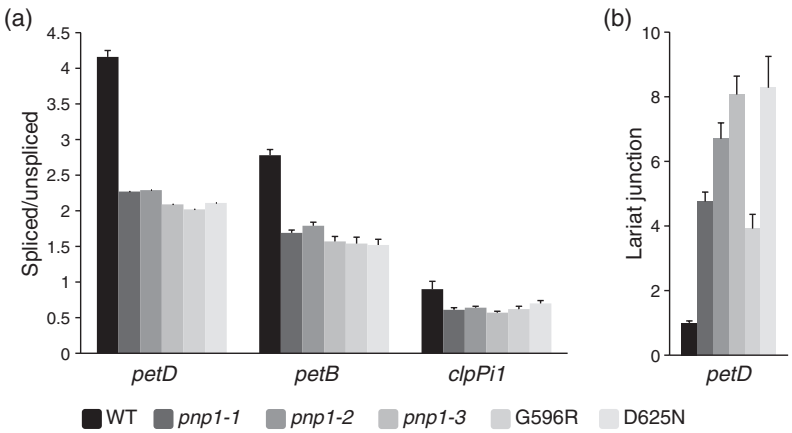

Figure 4. Effects of PNPase depletion on intron metabolism.
(a) Ratio of spliced to unspliced transcripts for *petD*, *petB* and *clpP* intron 1, as measured by Poisoned Primer Extension. Values shown for *petD* are the average of two experiments for the WT, and single samples for each of the null mutants. For *petB* and *clpPi1*, four samples for each mutant and eight WT samples were analyzed. Standard errors are shown.
(b) Relative amounts of *petD* intron fragments containing the lariat junction, measured by qRT-PCR. The results were normalized to actin, and standard error is shown. The data are derived from five biological replicates for each genotype.

These 5′-ends may represent sites of endonucleolytic cleavage, and would be expected to be impervious to PNPase activity, which has strict 3′ → 5′ polarity. In contrast, the WT and mutant had distinct clusters of 3′-ends, both located in Domain I. These were in the exon binding domain 2 (EBS2) for *pnp1-1*, and in a Domain I stem for the WT. These two clusters are separated by approximately 40 nt, which is consistent with the size difference of the cloned PCR products. The simplest interpretation is that PNPase normally completes degradation of the linearized intron, while occasionally stalling at the location marked by 3′-ends in the WT. On the other hand, PNPase seems to be required to degrade the intron sequences starting at EBS2.

Only homopolymeric poly(A) tails are detected in the pnp1-1 mutant

While investigating the 3′- and 5′-ends of the *petD* intron intermediate degradation products, we found three short non-encoded adenosine tails, as had previously been found for a small proportion of intron degradation products from other chloroplast genes (del Campo and Casano, 2008). The presence of these tails suggests that the *pnp1-1* mutant retains polyadenylation activity. To extend this analysis, we investigated the composition of poly(A) tails in the WT and *pnp1-1* using oligo(dT)-primed RT-PCR. As shown in Table 1, both homo- and heteropolymeric tails were found for the psbA mRNA in the WT, while only homopolymeric A-tails were present in *pnp1-1.* The heteropolymeric tails in bacteria and chloroplasts are generated by PNPase, while the homopolymeric tails are produced by poly(A) polymerase (PAP) (Slomovic *et al.*, 2008b). Therefore, the difference in composition suggests that in Arabidopsis chloroplasts, PNPase significantly contributes to the synthesis of heterogeneous poly(A) tails, whereas in its absence PAP activity creates homogeneous poly(A) tails. Similar features of polyadenylation by PAP and PNPase were initially described in *E. coli* (Mohanty and Kushner, 2000). Also of note was the fact that while the *psbA* 3′-end tails were longer in the WT compared with the mutant, 60% of the tails present in WT were heterogeneous at their 5′-ends, but terminated in 49–150-nt stretches of adenosines, suggesting that they may have been initiated by PNPase activity and elongated by PAP. The three 23S rRNA tails found from the WT were homogeneous poly(A), as were most of the tails from 16S rRNA. This contrasted with the rather heterogeneous tails of the *psbA* mRNA.

Arabidopsis cpPNPase *in vitro* activity is altered by point mutations

Data presented above for the TILLING mutants suggest that G596R and D625N lack activity, whereas P184L and S202N have diminished activity. The results for G596R were ambiguous, however, because the protein failed to accumulate in mutant tissue (Figure 1c). To support and extend these interpretations, we undertook an *in vitro* analysis of the WT enzyme and three point mutants, namely P184L, G596R, and a double mutant R176S–P184L. The double mutant was obtained fortuitously, but allowed us to define an important role for this region of the protein.

To avoid contamination by *E. coli* PNPase, the chloroplast proteins were expressed in bacterial *pnp* mutant cells, and purified to homogeneity (Figure 6a). We first tested the RNA-binding properties of these enzymes by UV crosslinking. As shown in Figure 6(b), the WT enzyme displayed a dissociation constant (K_d) of 22 nM, in the range of the 11 and 16.5 nM values for the *E. coli and* human mitochondrial enzymes (Portnoy *et al.*, 2008). Competition with polynucleotides showed that as previously reported for spinach cpPNPase (Yehudai-Resheff *et al.*, 2003), the Arabidopsis enzyme has a higher affinity for poly(U) and poly(A) than for poly(G) and poly(C) (data not shown). When the mutant enzymes were tested, P184L did not differ from the WT, R176S–P184L had a K_d value of 60 nM, and the G596R enzyme had no detectable RNA binding activity (Figure 6b).

As mentioned previously, cpPNPase is readily reversible *in vitro;* its degradation activity is stimulated by Pi addition,

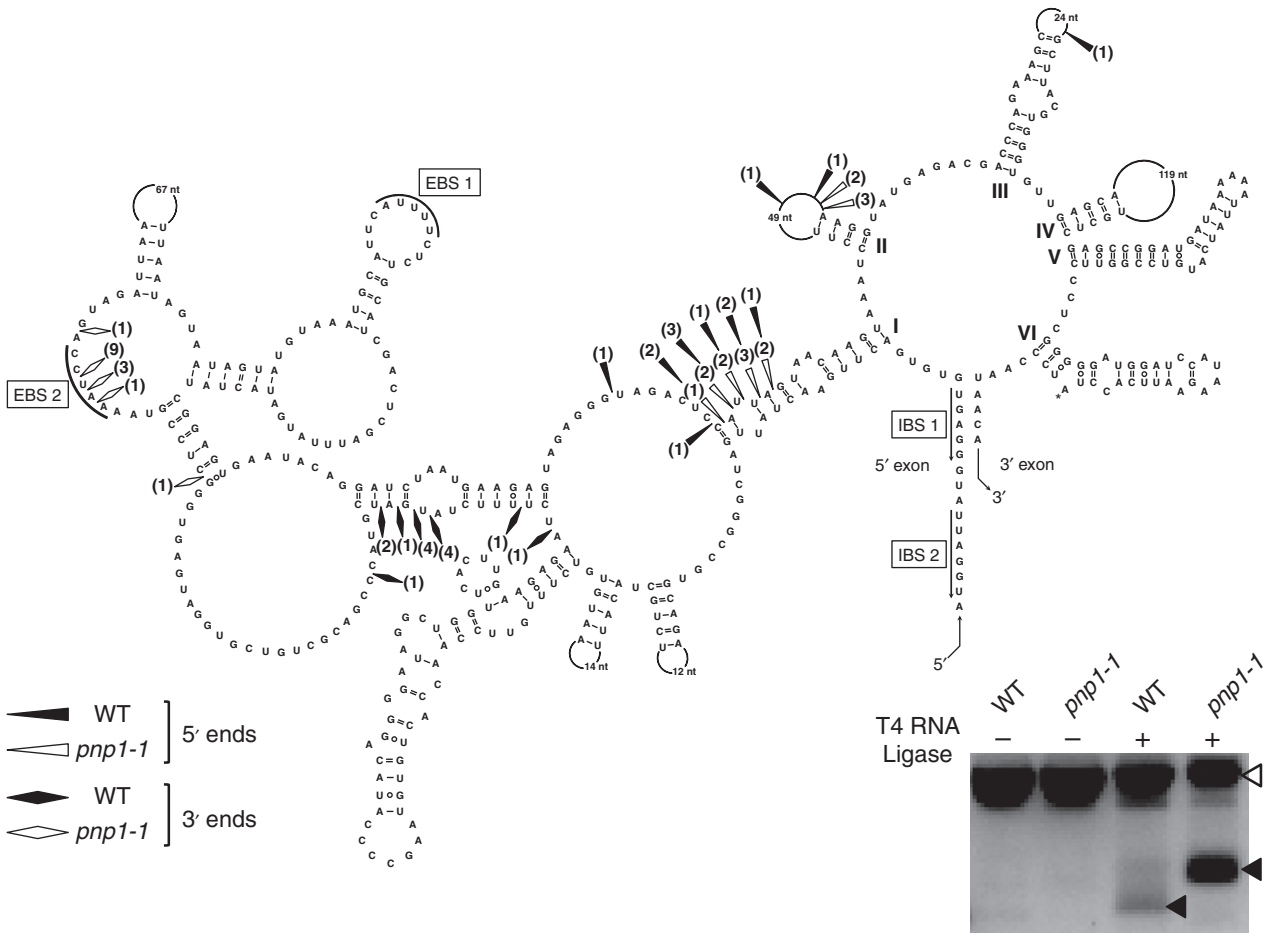

Figure 5. Intermediate degradation products of the *petD* intron.
Secondary structure of the Arabidopsis *petD* intron, based on Michel *et al.* (1989) EBS and IBS indicate exon and intron binding sites, respectively, and the Roman numerals I to VI denote particular intron domains. In the schematic, 5′-ends are represented by triangles and the 3′-ends by diamonds, with the WT and *pnp1-1* ends as filled and open symbols, respectively (see key at lower left). The numbers in parentheses correspond to the numbers of clones representing a particular end, out of 14 for the WT and 15 for *pnp1-1*. The 5′- and 3′-ends of the intermediates were mapped by sequencing cRT-PCR products (gel at lower right), with filled arrowheads indicating the products that were cloned and sequenced. The open arrowhead marks the intact intron, whose amplification is ligase-independent.

whereas polymerization occurs in the presence of NDPs. Figure 7 compares these activities for the WT and mutant enzymes. While the WT enzyme had robust polyadenylation and degradation activities (Figure 7a), G596R lacked both, consistent with its failure to detectably bind RNA *in vitro* (Figure 7b). P184L had reduced activity in both cases, as evidenced by the requirement for a higher Pi concentration to stimulate degradation, and lower production of poly(A) tails over time (Figure 7c). When the R176S–P184L double mutant was checked it had neither activity, suggesting that its weak RNA binding ability was insufficient to support catalysis under our experimental conditions (Figure 7b).

The significant effects of amino acid substitutions in the first core domain were somewhat unexpected, as it does not harbor the phosphorolytic site. In addition, while the intermediate catalytic activity of P184L was consistent with the RNA phenotypes observed by RNA gel blot analysis, the fact that the enzyme appeared to have normal RNA binding was counterintuitive. To explore this issue, we determined the quaternary structure of the recombinant enzymes. PNPase in *E. coli* is trimeric (Nurmohamed *et al.*, 2009), while spinach cpPNPase is most likely a dimer of trimers (Baginsky *et al.*, 2001). When the WT Arabidopsis enzyme was examined by standard or blue native gel electrophoresis, a hexameric form was identified (Figures S4a and 1c). This was also the case for the P184L and the R176S–P184L mutants, suggesting that their reduced catalytic activities could not be ascribed to altered quaternary structure. When the G596R mutant was analyzed, it migrated as a smear, suggesting a lack of discrete structure. The results for all enzymes were subsequently verified using column chromatography (Figure S4b). Therefore, a single amino acid change (G596R) can interfere with the ability to form the correct oligomeric structure, however the two-first core

Table 1 Poly(A) and poly(A)-rich sequences from WT and *pnp1-1*

Gene	Genotype	Tail length	Tail sequence	Position
psbA	WT	20–22	$A_{20–22}$	721
		41	$UA_{31}G_2A_7$	751
		74	$CAU_2GA_3UGAUCGAU_2GU_2G(UA)_2CUG_2(UC)_2U_3ACAU_2A_2UA_2U_5AC_2U_3AGC_2U_2A_{11}$	735
		81	$CUCAUC(CAU)_2A_3CA_2CU_2AC_2AGAU_2ACUA_{49}$	800
		113	$UCAUCU_4CU_2A_{101}$	753
		114	$A_{39}GA_{74}$	733
		129	$UGAC_2GUAUG_2U_3AC_2A_2U_2GC_2AGUACA_2UA_{97}$	729
		152	GGA_{150}	725
	pnp1-1	9–11	$A_{9–11}$	724
		11	A_{11}	681, 751, 759
		12–13	$A_{12–13}$	721
		13	A_{13}	758
		16–19	$A_{16–19}$	732
		19	A_{19}	754
		20–22	$A_{20–22}$	721
		22	A_{22}	723
		23–25	$A_{23–25}$	721
		28–29	$A_{28–29}$	815
23S rRNA	WT	10	A_{10}	2176
		13	A_{13}	1926, 2178
16S rRNA	WT	11	A_2GA_8	1346
		11	A_{11}	1439
		12	CA_{11}	1339
		14	A_{14}	1358
		17	A_{17}	1336
	pnp1-1	12	A_{12}	1325

RNA was used for oligo(dT)-primed RT-PCR for the indicated genes as described in Experimental procedures. The position of tail addition refers to Genbank accession number NC_000932.

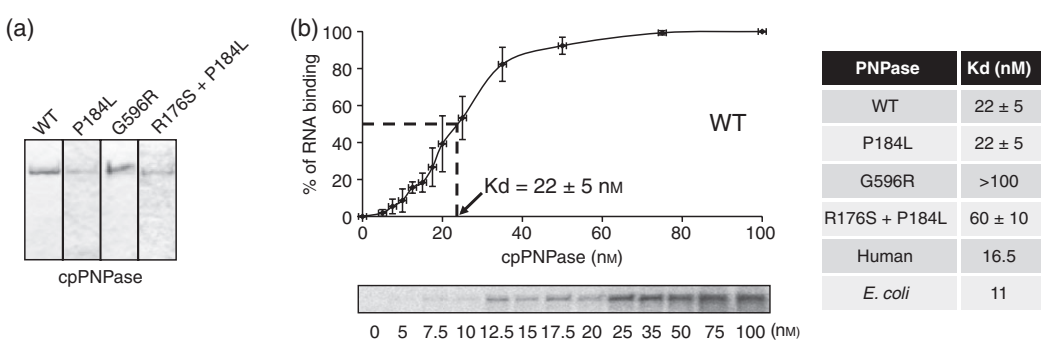

PNPase	Kd (nM)
WT	22 ± 5
P184L	22 ± 5
G596R	>100
R176S + P184L	60 ± 10
Human	16.5
E. coli	11

Figure 6. RNA binding properties of WT and mutant Arabidopsis cpPNPase.
(a) SDS-PAGE analysis of purified recombinant WT cpPNPase.
(b) Left, 10 ng WT cpPNPase was analyzed for RNA binding by UV crosslinking using the 3′-end [^{32}P]-*psbA* RNA and increasing amounts of the protein as indicated in the figure *inset*. The radioactive signals obtained in three independent experiments were averaged and plotted to determine the observed K_d. The K_d values for the WT and mutants are shown in the table to the right. Those for human and *E. coli* PNPases are taken from Portnoy *et al.* (2008).

domain mutants with altered activities appeared to assemble hexamers normally.

DISCUSSION

The many roles of chloroplast PNPase

Here we have used a variety of null mutants to dissect the roles of cpPNPase in RNA metabolism, supplemented by the analysis of recombinant proteins. Because the recombinant protein analyses are in agreement with the degree of disturbance for the RNA patterns, it is very likely that the observed RNA phenotypes are a direct consequence of reduced or abolished PNPase activity. The null mutants studied here also exhibit chlorosis in young leaves. An initial study of cpPNPase function relied on a co-suppressed line

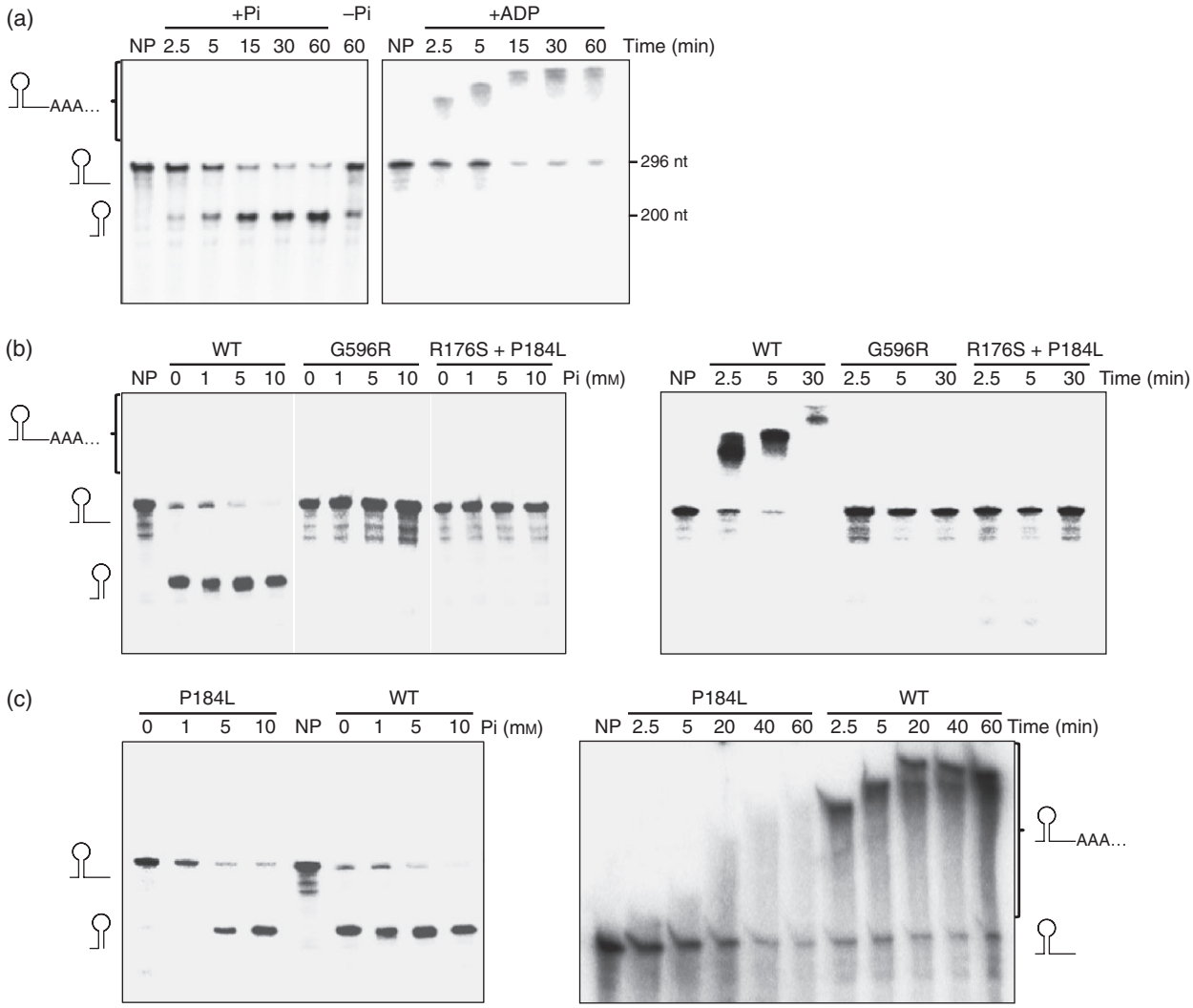

Figure 7. Analysis of recombinant cpPNPase for phosphorolytic and polymerization activities.
(a) A [^{32}P]-RNA of 296 nt corresponding to the 3′-end of the spinach *psbA* gene was used to analyze the phosphorolysis (left) and polymerization (right) activities of recombinant WT cpPNPase (50 ng for degradation and 100 ng for polymerization), in the presence of 5 mM phosphate or 2 mM ADP, respectively. After incubation, RNA was purified and analyzed by denaturing PAGE and imaging. NP – no protein added to the reaction; Pi – neither phosphate nor ADP were added and the incubation time was 60 min. The RNA molecules are schematically presented to the left and their lengths in nucleotides (nt) are shown at the right.
(b) Analysis as in panel (a), except the WT and two mutant enzymes were compared. Phosphorolysis activity (left) was analyzed by incubating the input RNA for 40 min with increasing Pi concentrations as shown; a time course was used for the polymerization assay (right).
(c) Analysis as in panel (b), except the WT and P184L enzymes were compared.

largely depleted for the enzyme, which did not express an obvious growth defect (Walter *et al.*, 2002), suggesting that even small amounts of cpPNPase are sufficient to confer a normal growth phenotype in Arabidopsis. Two TILLING mutants in the present study also have normal growth but display multiple RNA abnormalities. This situation leaves open the question of the proximal cause of young leaf chlorosis in *pnp* null mutants. Given that chloroplast gene expression is generally higher in young versus mature leaf chloroplasts (Baumgartner *et al.*, 1989), we suspect the chlorosis is a threshold effect related to RNA maturation rates or possibly translational efficiency. Indeed, several RNA phenotypes were much more pronounced in young, as compared with mature mutant leaves (Figure S5).

Our results reveal a remarkable number of gene expression steps in which PNPase can be implicated (Figure 8). These steps include 3′-end maturation (a and b), polynucleotide tail addition (c), tail-stimulated RNA degradation (d), and degradation of specific segments of linearized intron lariats (e and f). While many of these functions had previously been attributed to PNPase in various organisms, the breadth of its activities in a single context were not previously apparent. Clearly, PNPase is a central player in cpRNA metabolism.

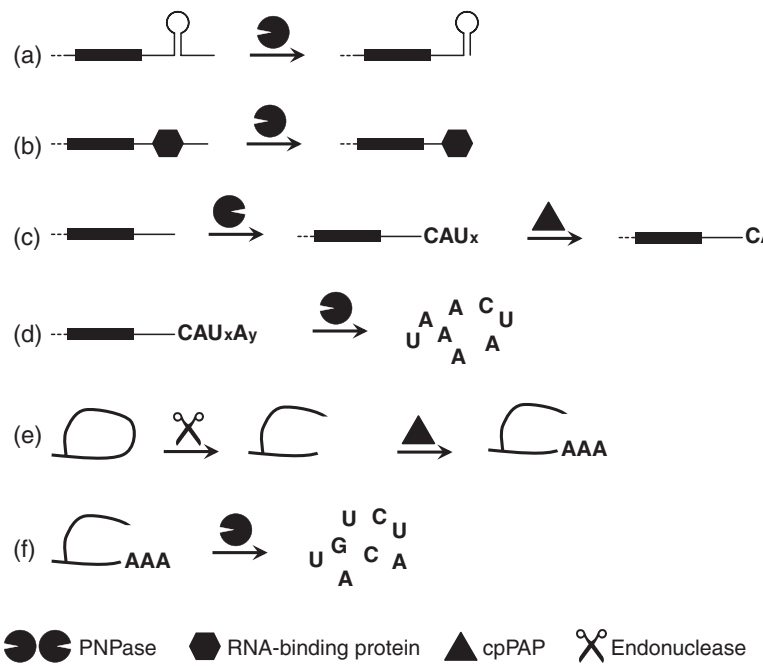

Figure 8. The various roles of PNPase in chloroplast RNA metabolism.
(a) PNPase resects the 3′-ends of pre-RNAs until it encounters a strong secondary structure.
(b) 3′-end maturation can also be defined by RNA-binding proteins such as those of the pentatricopeptide repeat family.
(c) 3′ polynucleotide tails that signal degradation may be formed by sequential activities of PNPase and a chloroplast poly(A) polymerase (cpPAP) activity, as shown here for *psbA*. *x* and *y* represent arbitrary numbers of heterogeneous nucleotides and adenosines, respectively.
(d) PNPase degrades polyadenylated transcripts in a 3′ → 5′ direction, after the polyadenylation step shown in (c).
(e) Excised intron lariats are hypothesized to be cleaved by an endoribonuclease, and the resulting product may be polyadenylated either by cpPAP as shown here, or by PNPase.
(f) The intermediate generated in (e) is subject to degradation by PNPase; thus, it accumulates to a high level in the *pnp* null mutants.

Both mRNAs and rRNAs depend on cpPNPase for correct maturation and degradation

One hallmark of cpPNPase mutant patterns is the accumulation of longer and more heterogeneous transcripts than the WT. Because chloroplast transcription termination is inefficient (Stern and Gruissem, 1987), 3′-end maturation requires post-transcriptional enzyme activity. cpPNPase was identified as an enzyme capable of catalyzing the 3′ to 5′ trimming of artificial precursors *in vitro* (Hayes *et al.*, 1996), and appears to partner with the exoribonuclease RNR1 to trim the 3′-end of 23S rRNA (Bollenbach *et al.*, 2005). Thus, in the case of monocistronic transcripts, the accumulating species may represent the products of stochastic termination followed by RNR1 trimming, or in some cases such as 23S rRNA, initial endonucleolytic cleavages at downstream tRNA or rRNA processing sites, followed by trimming. RNR1 belongs to the RNase II family whose members, like PNPase, are inhibited by strong RNA secondary structures (Spickler and Mackie, 2000). This or an RNA-binding protein (Figure 8b) may provide the basis for defining these transcript ends, or some may be generated directly by transcription termination.

A similar rationale cannot readily explain the numerous transcript abnormalities for the more complex gene clusters. A recently proposed model for transcript maturation in these contexts evokes endonucleolytic cleavages between cistrons, followed by 5′ → 3′ or 3′ → 5′ exonucleolytic trimming (Pfalz *et al.*, 2009), with the endpoints of mature transcripts defined by sequence-specific RNA-binding proteins or stem-loop structures (Figure 8a,b). Taking the *psbB* gene cluster as an example, we observed 3′ extensions for the three longest full length transcripts (bracketed in Figure 3b), which in the WT terminate at the 3′ stem-loop of *petD*, and these would be analogous to what was observed for *psbA* and *rbcL*. However, apart from this, the patterns were highly complex and sometimes quite diffuse (Figures 2 and S3). One interpretation is that these many transcripts represent endonucleolytic cleavage products by the chloroplast RNase E, which appears to be involved in polycistronic processing (Walter *et al.*, 2010). Because the chloroplast endonucleases CSP41 and RNase J may be partly redundant with RNase E (Pfalz *et al.*, 2009; Stern *et al.*, 2010), the species accumulating in the *pnp* mutants could also be cleavage products of these enzymes. The observed diffuseness could also represent the presence of polyadenylated species. Although it is difficult to measure quantitatively, our observation that it was much easier to obtain poly(A) tails using a *pnp* mutant rather than WT RNA (Table 1), hints that this is the case. This observation is also indirect evidence that PNPase has the major role in depleting poly(A)-tailed transcripts in the chloroplast.

PNPase and intron degradation

A surprising result was the accumulation of novel intron-containing fragments, along with a general decrease in splicing efficiency. We suspect that less efficient splicing is a pleiotropic effect of poor growth and/or chlorosis; chloroplast splicing is less pronounced in immature chloroplasts (Barkan, 1989) and is reduced when chloroplast translation is compromised (e.g. Jenkins *et al.*, 1997). The accumulation of intron fragments, however, suggests that PNPase plays an essential role in their recycling, and if these fragments

sequestered splicing factors, this could also reduce splicing efficiency. We showed that the most abundant *petD* species represents partial degradation of a lariat-containing structure, and it would not be surprising if other intron-containing species seen in *pnp* null mutants, such as for *petB* and *clpP*, had similar structures. Intron degradation has been little studied in chloroplasts, however chloroplasts do not appear to contain the lariat debranching activity that is present in other organisms (Vogel and Borner, 2002), suggesting that introns initially undergo an endonucleolytic cleavage (Figure 8e).

Importance of both PNPase core domains

Using TILLING, we were able to address roles of the duplicated RNase PH-like core domains of cpPNPase. PNPase crystal structures are available from *Streptomyces antibioticus* and *E. coli*, along with the archaeal exosome, which is very similar to PNPase (Lorentzen *et al.*, 2005; Nurmohamed *et al.*, 2009; Shi *et al.*, 2008; Symmons *et al.*, 2000). These studies, as well as others employing site-directed mutagenesis (Jarrige *et al.*, 2002), point to the second core domain as the active site. By analogy to the archaeal exosome, the first core domain would be expected to act as an accessory RNA-binding domain and function in trimer formation. In *S. antibioticus*, evidence also points to the first core domain as the site of synthesis of the SOS nucleotide pppGpp (Slomovic *et al.*, 2008b; Symmons *et al.*, 2000), as well as containing a binding site for pppGpp that represses enzyme activity (Gatewood and Jones, 2010). Mutagenesis of the human mitochondrial PNPase revealed the inhibition of activity when a first core amino acid was modified, disrupting the trimeric structure of the enzyme (Portnoy *et al.*, 2008).

In terms of the Arabidopsis cpPNPase, we obtained two mutations in or near the catalytic domain, and both plant lines exhibited phenotypes that were nearly indistinguishable from the null mutants. Because the G596R protein did not accumulate *in vivo* this is a trivial observation, although *in vitro* analysis confirmed that this protein is inactive. G596, which is located in the vicinity of the phosphorolytic active site, is conserved in all PNPases (Yehudai-Resheff *et al.*, 2003). We suspect that G596R fails to fold correctly, perhaps as a consequence of its inability to bind phosphate, and is thus marked for degradation. The D625N mutant accumulated at least WT levels of protein, and therefore must be inactive. Indeed, D625 is located in the catalytic site, functions in phosphorolysis, and is conserved in virtually all PNPases from bacteria, organelles as well as the equivalent subunit, Rrp41, of the archaeal exosome. Accordingly, mutagenesis of D625 in other studies also inactivated the enzyme (Jarrige *et al.*, 2002; Lorentzen *et al.*, 2005; Portnoy *et al.*, 2008).

The original TILLING screen generated a large number of mutants, of which those with non-neutral mutations in conserved residues among organellar PNPases were selected for further analysis. In spite of this screen, only two mutations in the first core domain conferred detectable RNA phenotypes. P184L showed a mixture of WT and mutant bands for most RNAs analyzed, whereas S202N only exhibited aberrant patterns for the *psbB* gene cluster, in particular the *petD* intron, as well as the gene cluster containing *psbD-psbC* (Figure S3). Because only a subset of chloroplast genes were analyzed, it is likely that S202N affects other transcripts, presumably those that are particularly dependent on PNPase for their processing or degradation. Although the S202N mutation appeared to result in reduced cpPNPase accumulation (Figure 1c), there was no effect on abundant transcripts such as 23S rRNA, suggesting that altered S202N activity rather than its overall abundance, conferred the observed phenotypes. Unfortunately, when expressed in bacteria, this mutant was not obtained as a soluble protein and therefore could not be analyzed *in vitro* for phosphorolysis activity and RNA binding.

The importance of the first core domain for PNPase activity is also evident from the *in vitro* analyses of P184L and R176S–P184L. The double mutant lacks phosphorolysis activity and binds RNA with less affinity compared with the WT protein. These two amino acids are far from the phosphorolytic site, but their substitution is predicted to interrupt the α-helix structure they are part of. It is possible that this disruption in turn causes conformational changes manifested in RNA affinity below the threshold required for activity. As shown by the *in vitro* analysis, the reduced RNA affinity leads to inability of the RNA to enter the phosphorolytic site, and hence a complete inhibition of activity. On the other hand, P184L displays similar RNA affinity to the WT, but intermediate phosphorolytic activity between the WT and the inactive or null mutants. In this case, we hypothesize that the conformational change induced by the interruption of the α-helix still enables RNA binding, and thus reduced but not eliminated enzyme activity. Furthermore, these mutations are located in the vicinity of the *E. coli* PNPase citrate-binding site (Nurmohamed *et al.*, 2009), where modulation of PNPase activity is achieved (Nurmohamed *et al.*, 2010). Indeed, PNPase catalytic activity appears to involve changes in the quaternary structure (S. Hardwick and B. Luisi, University of Cambridge, Cambridge, UK, personal communication), which could be relevant to the phenotypes we observed for the first core domain mutants.

We considered that these first core domain mutations might directly impose changes in the oligomeric structure of the enzyme, as shown before for the trimeric human PNPase (Portnoy *et al.*, 2008). As previously suggested (Symmons *et al.*, 2002), changes in the oligomeric structure might alter processivity, as indeed can be inferred from the polyadenylation activity of the P184L mutant (Figure 7). However, both first core domain mutants still formed hexamers,

leaving unclear the reason for the formation of hexameric PNPase in the chloroplast, as compared with the trimers found in bacteria and human mitochondria. Mutants able to form trimers, but not hexamers, would be valuable in this regard.

EXPERIMENTAL PROCEDURES

Plant material and growth conditions

Arabidopsis thaliana experiments used ecotype Col-0. Plants were grown on soil under long days (16 h light/8 h dark) at 22°C. The Arabidopsis *pnp1-1* and *pnp1-2* T-DNA insertion mutants were previously described (Marchive *et al.*, 2009). The TILLING mutants (Till *et al.*, 2003) were obtained using gene-specific primer pairs (5′-GGAGCGATTCTCAGCTGTAGG-3′, 5′-CATATTTCTTTGCTAAA-ACTT-3′; 5′-TTGGAGGATGAAGACGAG-3′, 5′-TCCATTATCTC-TAAAGTAATTCCTCCT-3′) for the 1st and the 2nd core domains, respectively. Any background mutations caused by the EMS treatment were removed by four backcrosses to Col-0 WT. Genotyping used the DCAPS FINDER 2.0 program (Neff *et al.*, 2002).

RNA analysis

Total RNA was isolated and analyzed as described (Marchive *et al.*, 2009). Equal loading of 0.5 μg of total RNA was achieved by preparing a 10 μg stock of RNA mixed with loading buffer and visually adjusting the amount of rRNA loaded for each sample. The RNA stock was denatured once at 65°C, stored at –80°C and thawed on ice for each gel loading. Poisoned Primer Extension was done according to Asakura and Barkan (2006), qRT-PCR as described by Marchive *et al.* (2009), using 2 μg of total RNA, and cRT-PCR as described previously by Perrin *et al.* (2004b). Poly(A) tails for the *psbA* transcript were characterized by oligo(dT)-primed RT-PCR according to Slomovic *et al.* (2008a). All primers are listed in Table S1.

Protein analysis

Leaves from 4- to 5-week-old plants grown under long day conditions were harvested and plastids were enriched according to van Wijk *et al.* (2007) from steps 1 through 6. Once the chloroplasts were pelleted, soluble proteins were extracted in a native soluble protein extraction buffer (100 mM Tris. pH 8.0, 18% sucrose, 40 mM β-mercaptoethanol and 1 mM phenylmethyl sulfonyl fluoride). Proteins were separated in a NativePAGE™ 3–12% Bis-Tris Gel (Invitrogen BN2011BX10, http://invitrogen.com) and transferred to an Immun-Blot™ PVDF membrane, according to the protocol of the NativePAGE™ Novex® Bis-Tris Gel System (XCell SureLock™; Invitrogen). The membrane was blocked in TBS-T + 5% milk for 1 h at room temperature before adding 1:3000 PNPase antibody and agitating at 4°C overnight, prior to detection.

Production of recombinant PNPase and its mutated versions

The cDNA encoding the mature protein was amplified from leaf RNA (for primers see Table S1). Point mutations were introduced into the WT protein using the QuikChange™ site-directed mutagenesis kit (Stratagene Inc., http://www.genomics.agilent.com), and DNA sequences were verified to exclude PCR-induced mutations. In this way, the R176S mutation was discovered. For expression in *E. coli*, PCR products were inserted into Pet20b, which encodes a C-terminal His_6 tag. The proteins were expressed in ENS134–3, which lacks endogenous PNPase (Lopez *et al.*, 1999), kindly obtained from Marc Dreyfus (Ecole Normale Supérieure, http://www.ens.fr). The proteins were purified as previously described (Portnoy *et al.*, 2008), to the stage of a single Coomassie blue-stained band as visualized by SDS-PAGE (Figure 6a). The mutant S202N was not obtained as a soluble protein and therefore was not further analyzed. No contaminating *E. coli* RNase II or RNase E was detected by immunoblot. In order to analyze its oligomeric form, purified PNPase was fractionated by Superdex 200 size exclusion column chromatography (Portnoy *et al.*, 2008). For antibody production, 1.5 mg of recombinant protein was injected into rabbits (Sigma, Inc, http://www.sigmaaldrich.com).

Polyadenylation, degradation assays and UV-crosslinking

The plasmid used for the *in vitro* synthesis of the RNA corresponding to the 3′-end of the spinach chloroplast *psbA* has been described, as well as the procedures for assays of polyadenylation and degradation activities of the recombinant proteins (Yehudai-Resheff *et al.*, 2003). Briefly, [^{32}P]-RNA was incubated with the corresponding proteins (50 ng for degradation; 100 ng for polymerization) in Buffer E with the addition of Pi for degradation assay, or with ADP when polyadenylation activity was to be monitored. Following incubation, the RNA was isolated and analyzed by denaturing PAGE and autoradiography. UV-crosslinking of proteins to radiolabeled RNA was performed as previously described (Portnoy *et al.*, 2008). For the competition assay, the protein was first mixed with the ribohomopolymers and then the radiolabeled RNA was added.

Arabidopsis seed stocks

SALK_013306 (*pnp1-1*), SALK_070705 (*pnp1-2*), CS85511 (P184L), CS87183 (*pnp1-3*), CS86422 (S202N), CS90749 (A213T), CS93797 (L223F), CS93456 (A263V), CS85733 (G524R), CS93798 (P529L), CS92335 (P589S), CS91942 (G596R), CS93256 (D625N).

ACKNOWLEDGEMENTS

This work was supported by awards from the Binational Agricultural Research and Development Fund (IS-4152–08C) and the Binational Science Foundation (2009253) to G.S. and D.B.S. We thank Shiri Levy and Shimyn Slomovic for help with the cloning of the Arabidopsis PNPase and analysis of the poly(A) tails, respectively, and Alice Barkan for extensive discussions regarding cpPNPase function.

SUPPORTING INFORMATION

Additional Supporting Information may be found in the online version of this article:

Figure S1. Gel electrophoresis to examine ribosomal RNAs.

Figure S2. RNA gel blot hybridization for two monocistronic mRNAs, *rbcL* and *psbA* and the dicistronic *atpB*/*E* mRNA.

Figure S3. RNA phenotypes of PNPase mutants.

Figure S4. Quaternary structures of recombinant PNPases.

Figure S5. RNA gel blot to compare mature and young leaves.

Table S1. Sequences of oligonucleotide primers used in this study.

Please note: As a service to our authors and readers, this journal provides supporting information supplied by the authors. Such materials are peer-reviewed and may be re-organized for online delivery, but are not copy-edited or typeset. Technical support issues arising from supporting information (other than missing files) should be addressed to the authors.

REFERENCES

Asakura, Y. and Barkan, A. (2006) Arabidopsis orthologs of maize chloroplast splicing factors promote splicing of orthologous and species-specific group II introns. *Plant Physiol.* **142**, 1656–1663.

Baginsky, S., Shteiman-Kotler, A., Liveanu, V., Yehudai-Resheff, S., Bellaoui, M., Settlage, R.E., Shabanowitz, J., Hunt, D.F., Schuster, G. and Gruissem, W. (2001) Chloroplast PNPase exists as a homo-multimer enzyme complex that is distinct from the *Escherichia coli* degradosome. *RNA*, **7**, 1464–1475.

Barkan, A. (1989) Tissue-dependent plastid RNA splicing in maize: transcripts from four plastid genes are predominantly unspliced in leaf meristems and roots. *Plant Cell*, **1**, 437–446.

Baumgartner, B.J., Rapp, J.C. and Mullet, J.E. (1989) Plastid transcription activity and DNA copy number increase early in barley chloroplast development. *Plant Physiol.* **89**, 1011–1018.

Bollenbach, T.J., Lange, H., Gutierrez, R., Erhardt, M., Stern, D.B. and Gagliardi, D. (2005) RNR1, a 3′–5′ exoribonuclease belonging to the RNR superfamily, catalyzes 3′ maturation of chloroplast ribosomal RNAs in *Arabidopsis thaliana*. *Nucleic Acids Res.* **33**, 2751–2763.

del Campo, E.M. and Casano, L.M. (2008) Degradation of plastid unspliced transcripts and lariat group II introns. *Biochimie*, **90**, 474–483.

Chen, H.W., Rainey, R.N., Balatoni, C.E. *et al.* (2006) Mammalian PNPase is an intermembrane space ribonuclease that maintains mitochondrial homeostasis. *Mol. Cell. Biol.* **26**, 8475–8487.

Deutscher, M.P. (1993) Promiscuous exoribonucleases of *Escherichia coli*. *J. Bacteriol.* **175**, 4577–4583.

Gatewood, M.L. and Jones, G.H. (2010) (p)ppGpp Inhibits polynucleotide phosphorylase from *Streptomyces* but not from *Escherichia coli* and increases the stability of bulk mRNA in *Streptomyces coelicolor*. *J. Bacteriol.* **192**, 4275–4280.

Grunberg-Manago, M. and Ochoa, S. (1955) Enzymatic synthesis and breakdown of polynucleotides; polynucleotide phosphorylase. *J. Am. Chem. Soc.* **77**, 3165–3166.

Hayes, R., Kudla, J., Schuster, G., Gabay, L., Maliga, P. and Gruissem, W. (1996) Chloroplast mRNA 3′-end processing by a high molecular weight protein complex is regulated by nuclear encoded RNA binding proteins. *EMBO J.* **15**, 1132–1141.

Holec, S., Lange, H., Kuhn, K., Alioua, M., Borner, T. and Gagliardi, D. (2006) Relaxed transcription in Arabidopsis mitochondria is counterbalanced by RNA stability control mediated by polyadenylation and polynucleotide phosphorylase. *Mol. Cell. Biol.* **26**, 2869–2876.

Jarrige, A., Brechemier-Baey, D., Mathy, N., Duche, O. and Portier, C. (2002) Mutational analysis of polynucleotide phosphorylase from *Escherichia coli*. *J. Mol. Biol.* **321**, 397–409.

Jenkins, B.D., Kulhanek, D.J. and Barkan, A. (1997) Nuclear mutations that block group II RNA splicing in maize chloroplasts reveal several intron classes with distinct requirements for splicing factors. *Plant Cell*, **9**, 283–296.

Komine, Y., Kwong, L., Anguera, M.C., Schuster, G. and Stern, D.B. (2000) Polyadenylation of three classes of chloroplast RNA in *Chlamydomonas reinhardtii*. *RNA*, **6**, 598–607.

Lopez, P.J., Marchand, I., Joyce, S.A. and Dreyfus, M. (1999) The C-terminal half of RNase E, which organizes the *Escherichia coli* degradosome, participates in mRNA degradation but not rRNA processing *in vivo*. *Mol. Microbiol.* **33**, 188–199.

Lorentzen, E., Walter, P., Fribourg, S., Evguenieva-Hackenberg, E., Klug, G. and Conti, E. (2005) The archaeal exosome core is a hexameric ring structure with three catalytic subunits. *Nat. Struct. Mol. Biol.* **12**, 575–581.

Marchive, C., Yehudai-Resheff, S., Germain, A., Fei, Z., Jiang, X., Judkins, J., Wu, H., Fernie, A.R., Fait, A. and Stern, D.B. (2009) Abnormal physiological and molecular mutant phenotypes link chloroplast polynucleotide phosphorylase to the phosphorus deprivation response in Arabidopsis. *Plant Physiol.* **151**, 905–924.

Michel, F., Umesono, K. and Ozeki, H. (1989) Comparative and functional anaotmy of group II catalytic introns–a review. *Gene*, **82**, 5–30.

Mohanty, B.K. and Kushner, S.R. (2000) Polynucleotide phosphorylase functions both as a 3′ to 5′ exonuclease and a poly(A) polymerase in *Escherichia coli*. *Proc. Natl Acad. Sci. USA*, **97**, 11966–11971.

Neff, M.M., Turk, E. and Kalishman, M. (2002) Web-based primer design for single nucleotide polymorphism analysis. *Trends Genet.* **18**, 613–615.

Nurmohamed, S., Vaidialingam, B., Callaghan, A.J. and Luisi, B.F. (2009) Crystal structure of *Escherichia coli* polynucleotide phosphorylase core bound to RNase E, RNA and manganese: implications for catalytic mechanism and RNA degradosome assembly. *J. Mol. Biol.* **389**, 17–33.

Nurmohamed, S., Vincent, H., Titman, C., Chandran, V., Pears, M., Du, D., Griffin, J., Callaghan, A. and Luisi, B. (2010) Polynucleotide phosphorylase activity may be modulated by metabolites in *Escherichia coli*. *J. Mol. Chem.* **286**, 14315–14323.

Perrin, R., Lange, H., Grienenberger, J.M. and Gagliardi, D. (2004a) AtmtPNPase is required for multiple aspects of the 18S rRNA metabolism in *Arabidopsis thaliana* mitochondria. *Nucleic Acids Res.* **32**, 5174–5182.

Perrin, R., Meyer, E.H., Zaepfel, M., Kim, Y.J., Mache, R., Grienenberger, J.M., Gualberto, J.M. and Gagliardi, D. (2004b) Two exoribonucleases act sequentially to process mature 3′-ends of *atp9* mRNAs in Arabidopsis mitochondria. *J. Biol. Chem.* **279**, 25440–25446.

Pfalz, J., Bayraktar, O.A., Prikryl, J. and Barkan, A. (2009) Site-specific binding of a PPR protein defines and stabilizes 5′ and 3′ mRNA termini in chloroplasts. *EMBO J.* **28**, 2042–2052.

Portnoy, V., Palnizky, G., Yehudai-Resheff, S., Glaser, F. and Schuster, G. (2008) Analysis of the human polynucleotide phosphorylase (PNPase) reveals differences in RNA binding and response to phosphate compared to its bacterial and chloroplast counterparts. *RNA*, **14**, 297–309.

Sauret-Gueto, S., Botella-Pavia, P., Flores-Perez, U., Martinez-Garcia, J.F., San Roman, C., Leon, P., Boronat, A. and Rodriguez-Concepcion, M. (2006) Plastid cues posttranscriptionally regulate the accumulation of key enzymes of the methylerythritol phosphate pathway in Arabidopsis. *Plant Physiol.* **141**, 75–84.

Schuster, G. and Stern, D. (2009) RNA polyadenylation and decay in mitochondria and chloroplasts. *Prog. Mol. Biol. Transl. Sci.* **85**, 393–422.

Schweer, J., Loschelder, H. and Link, G. (2006) A promoter switch that can rescue a plant sigma factor mutant. *FEBS Lett.* **580**, 6617–6622.

Shi, Z., Yang, W.Z., Lin-Chao, S., Chak, K.F. and Yuan, H.S. (2008) Crystal structure of *Escherichia coli* PNPase: central channel residues are involved in processive RNA degradation. *RNA*, **14**, 2361–2371.

Slomovic, S. and Schuster, G. (2008) Stable PNPase RNAi silencing: its effect on the processing and adenylation of human mitochondrial RNA. *RNA*, **14**, 310–323.

Slomovic, S., Portnoy, V. and Schuster, G. (2008a) Detection and characterization of polyadenylated RNA in Eukarya, Bacteria, Archaea, and organelles. *Methods Enzymol.* **447**, 501–520.

Slomovic, S., Portnoy, V., Yehudai-Resheff, S., Bronshtein, E. and Schuster, G. (2008b) Polynucleotide phosphorylase and the archaeal exosome as poly(A)-polymerases. *Biochim. Biophys. Acta*, **1779**, 247–255.

Spickler, C. and Mackie, G.A. (2000) Action of RNase II and polynucleotide phosphorylase against RNAs containing stem-loops of defined structure. *J. Bacteriol.* **182**, 2422–2427.

Stern, D.B. and Gruissem, W. (1987) Control of plastid gene expression: 3′ inverted repeats act as mRNA processing and stabilizing elements, but do not terminate transcription. *Cell*, **51**, 1145–1157.

Stern, D.B., Goldschmidt-Clermont, M. and Hanson, M.R. (2010) Chloroplast RNA metabolism. *Annu. Rev. Plant Biol.* **61**, 125–155.

Symmons, M.F., Jones, G.H. and Luisi, B.F. (2000) A duplicated fold is the structural basis for polynucleotide phosphorylase catalytic activity, processivity, and regulation. *Structure Fold Des.* **8**, 1215–1226.

Symmons, M.F., Williams, M.G., Luisi, B.F., Jones, G.H. and Carpousis, A.J. (2002) Running rings around RNA: a superfamily of phosphate-dependent RNases. *Trends Biochem. Sci.* **27**, 11–18.

Till, B.J., Reynolds, S.H., Greene, E.A. *et al.* (2003) Large-scale discovery of induced point mutations with high-throughput TILLING. *Genome Res.* **13**, 524–530.

Vogel, J. and Borner, T. (2002) Lariat formation and a hydrolytic pathway in plant chloroplast group II intron splicing. *EMBO J.* **21**, 3794–3803.

Walter, M., Kilian, J. and Kudla, J. (2002) PNPase activity determines the efficiency of mRNA 3′-end processing, the degradation of tRNA and the extent of polyadenylation in chloroplasts. *EMBO J.* **21**, 6905–6914.

Walter, M., Piepenburg, K., Schöttler, M.A., Petersen, K., Kahlau, S., Tiller, N., Drechsel, O., Weingartner, M., Kudla, J. and Bock, R. (2010) Knockout of the plastid RNase E leads to defective RNA processing and chloroplast ribosome deficiency. *Plant J.* **64**, 851–863.

Wang, G., Chen, H.W., Oktay, Y. *et al.* (2010) PNPase regulates RNA import into mitochondria. *Cell*, **142**, 456–467.

van Wijk, K.J., Peltier, J.B. and Giacomelli, L. (2007) Isolation of chloroplast proteins from *Arabidopsis thaliana* for proteome analysis. *Methods Mol. Biol.* **355**, 43–48.

Yehudai-Resheff, S., Hirsh, M. and Schuster, G. (2001) Polynucleotide phosphorylase functions as both an exonuclease and a poly(A) polymerase in spinach chloroplasts. *Mol. Cell. Biol.* **21**, 5408–5416.

Yehudai-Resheff, S., Portnoy, V., Yogev, S., Adir, N. and Schuster, G. (2003) Domain analysis of the chloroplast polynucleotide phosphorylase reveals discrete functions in RNA degradation, polyadenylation, and sequence homology with exosome proteins. *Plant Cell*, **15**, 2003–2019.

Yehudai-Resheff, S., Zimmer, S.L., Komine, Y. and Stern, D.B. (2007) Integration of chloroplast nucleic acid metabolism into the phosphate deprivation response in *Chlamydomonas reinhardtii*. *Plant Cell*, **19**, 1023–1038.

Zghidi, W., Merendino, L., Cottet, A., Mache, R. and Lerbs-Mache, S. (2007) Nucleus-encoded plastid sigma factor SIG3 transcribes specifically the *psbN* gene in plastids. *Nucleic Acids Res.* **35**, 455–464.

Zimmer, S.L., Schein, A., Zipor, G., Stern, D.B. and Schuster, G. (2009) Polyadenylation in Arabidopsis and *Chlamydomonas* organelles: the input of nucleotidyltransferases, poly(A) polymerases and polynucleotide phosphorylase. *Plant J.* **59**, 88–99.